Postprint of: Janik M., Głowacki M., Sawczak M., Wcisło A., Niedziałkowski P., Jurak K., Ficek M., Bogdanowicz R., Poly-L-Lysine-functionalized fluorescent diamond particles: pH triggered fluorescence enhancement via surface charge modulation, MRS BULLETIN, Vol. 47 (2022), pp. 1011–1022

Poly-L-Lysine-functionalized fluorescent diamond particles: pH triggered fluorescence enhancement via surface charge modulation

Monika Janik [1,2,*], Maciej J. Głowacki [1], Mirosław Sawczak [3], Anna Wcisło [4], Paweł Niedziałkowski [4], Kacper Jurak[5], Mateusz Ficek [1] and Robert Bogdanowicz [1]

[1] Department of Metrology and Optoelectronics, Faculty of Electronics, Telecommunications and Informatics, Gdańsk University of Technology, 11/12 Gabriela Narutowicza Street, 80-233 Gdańsk, Poland

[2] Institute of Microelectronics and Optoelectronics, Warsaw University of Technology, 75 Koszykowa Street, 00-662 Warsaw, Poland

[3] Center for Plasma and Laser Engineering, The Szewalski Institute of Fluid-Flow Machinery, Polish Academy of Sciences, 14 Józefa Fiszera Street, 80-231 Gdańsk, Poland

[4] Department of Analytical Chemistry, Faculty of Chemistry, University of Gdańsk, 63 Wita Stwosza Street, 80-308 Gdańsk, Poland

[5] Department of Electrochemistry, Corrosion and Materials Engineering, Faculty of Chemistry, Gdańsk University of Technology, 11/12 Gabriela Narutowicza Street, Gdańsk 80-233, Poland

*Address correspondence to monika.janik@pg.edu.pl

Abstract

Recently, the interest in applying fluorescent diamond particles (FDPs) containing nitrogen-vacancy (NV) centers for enhancing the mechanical and chemical properties of some materials, biological imaging, and sensing is expanding rapidly. The unique properties of NV- centers such as intensive, time-stable fluorescence, and an electron spin, which exhibits long coherence time and may be manipulated using external stimuli, such as pH, make them a perfect candidate for a quantum-effect-based sensing platform. However, monitoring of the local changes with the use of the nonmodified diamond particles has certain limitations, therefore, to enhance their sensing properties, in this work, the covalent functionalization of the FDPs' surfaces with poly-L-Lysine (pLys) (NV-pLys) is presented. The FDPs' surface is functionalized in an anhydrous environment, and successful attachment is confirmed by Fourier-transform infrared spectroscopy (FT-IR). As the pLys undergoes pH-triggered changes of conformation, it also induced changes in the diamonds' surface charge, therefore modulating the fluorescence, and finally as a result enhanced NV-pLys pH-sensitivity. Further investigation of the zeta potential, particle size, and contact angle reveals remarkable colloidal stability and superior wettability of the NV-pLys over a wide range of pH what also may significantly affect NV-pLys biocompatibility. These findings open new possibilities for the construction of biocompatible, stable, and highly sensitive nanosensors.

Key words: nanodiamonds, nitrogen-vacancy centers, poly-L-Lysine; surface functionalization; pH measurements

1. Introduction

Fluorescent diamond particles (FDPs) containing negatively charged nitrogen-vacancy (NV^-) color centers due to their distinctive nature are widely used in many disciplines including material science, energy, environment, and biomedicine [1]. NV^- centers exhibit strong and stable fluorescence. Moreover, the electronic spin of these centers is sensitive to magnetic field [2,3] and temperature [4,5]. Diamond particles are characterized by biological and chemical inertness [1], as well as large and easy-to-functionalize surfaces [6]. All these features make FDPs widely used for optical detection and imaging of biological matter [7, 8]. They were being used alone – in a form of suspension - or as an addition for materials such as bone implants [9,10]. Fluorescent defects in the crystal lattices of the diamonds are highly photostable; however, they may change their chemical and optical properties according to the changes in a highly complex biological environment around the crystal.

One of the key factors influencing the applicability of the diamonds containing NV^- centers to biosensing is the pH of surrounding media. Since oscillations of NV^- electron spin are used to determine external magnetic fields, their pH dependency is crucial for the accuracy and the resolution of the measurements. A particular pH change, in turn, is associated with chemical and biological events of interest [11]. For example, the values of both the extracellular and intracellular pH of tumors, are acidic in the range of 6.4–7.0, while for healthy cells (brain tissues, subcutaneous tissues, etc.) pH values are found in the range of 7.2–7.5 [12]. A local drop in pH is also a common feature of inflammation of the soft as well as hard tissues around, e.g., bone implants [13]. Therefore, it becomes increasingly important to find and ascertain the aspects of NV^- centers' behavior in a variety of environments before utilizing them as biosensors, or imaging agents because regardless of pH, the fluorescence of NV^- centers must be intensive enough to be easily detected inside different biological systems. The NV^- center provides several readout options. First, optical measurement of spin-lattice relaxation time of NV^- centers [14,15] and spectral shifts of the NV zero-phonon lines (ZPLs) [16]. Some of the approaches also included the connection of FDPs with a smart responsive polymer transducer/surface functionalization which has been used for pH measurements [15,17,18] which extended the measured pH range.

Alongside exploring the issue of the impact of pH on NV^-, it is crucial to circumvent the negative aspects associated with FDPs toxic behavior and interference with cell activities. Besides the biocompatibility, the crystal should be precisely designed and functionalized in a way to control properties such as rigidity, surface charge, topography, and wettability, which, in turn, control and affect cellular functions and behavior. Most studies have shown that hydrophilic surfaces tend to enhance the early stages of cell adhesion, proliferation, differentiation, or bone mineralization compared to hydrophobic ones [19]. Although the majority of published works report FDPs as biocompatible based on cell [20] and animal [21] studies, several recent works document their toxic effects both *in vitro* [22] as well as *in vivo* [23,24]. Reported findings indicate that FDPs' biocompatibility should not be overgeneralized. An FDPs' biological response strongly depends on their size, shape [25], as well as functional groups on their surface. However, since they have tailored surface chemistry, their toxicity partially can be managed through surface modification with biological molecules.

Recent studies [26] have shown the advantages of surface modification with poly-L-Lysine (pLys) since it is highly efficient, biocompatible, widely available, and promotes cellular internalization. pLys is the polymeric form of the naturally occurring amino acid L-Lysine and its degree of polymerization can be easily controlled by obtaining different shapes and molecular weights. To date, the pLys-functionalization has been utilized on the FDPs to control aggregation and ensure long-term stability of the diamonds' dispersions [27]; provide noncovalent surface amination [28]; enhance their biocompatibility[20], and prepare their surface for gene carrying [29]. The FDPs' surface can be modified with pLys in two ways. Firstly, using noncovalent adsorption on the particle's surface through electrostatic interactions and van der Waals forces [28]. Although it is easy to achieve, it may lead to desorption and competitive displacement of active moieties in a complex biological environment, therefore compromising the long-term stability of the system. Secondly, a covalent conjugation – which overcomes deficiency – by permanent immobilization of the pLys on the surface to create a controlled and relatively stable functionalized system [20]. Moreover, owing to its conformation, pLys is also an excellent, yet probably the simplest model of peptide which undergoes a remarkable pH-induced conformational transition. At acidic or neutral conditions, pLys chains adopt a relaxed, random coil conformation, while adopting α-helix conformation owing to the deprotonation of lysine residues of pLys under alkaline conditions. Figure 1 presents the explanatory model of pLys conformations depending on pH of the medium.

In this work, we show that the level of the fluorescence signal emitted by NV^- defects embedded in the FDP structure depends on external pH. However, monitoring of pH changes using a mechanism of charge transfer between nitrogen-vacancy centers is limited with nonmodified, carboxylated FDPs (NV-COOH). To widen the measurable pH range of the particles their surface has been covalently functionalized with the use of pLys (NV-pLys). Considering pLys properties, the functionalization modulated the FDPs' surface charge, therefore enabling monitoring of the pH in a broader range. Noteworthy, NV-pLys demonstrated also remarkable stability over a wide range of pH and superior wettability. This may significantly improve NV-pLys biocompatibility for a variety of biomedical applications, as hydrophilicity influences biocompatibility.

2. Methods

Materials and Chemicals: Carboxylated, fluorescent diamond particles (labeled NV-COOH in this study) with an average particle size of ≈750 nm have been purchased from Adámas Nanotechnologies, USA. Poly-L-Lysine 0.1 % (w/v) solution in H_2O, N,N-Dimethylformamide (DMF), hydrochloric acid (HCl), sodium hydroxide (NaOH), and N,N'-Diisopropylcarbodiimide (DIC) have been purchased from Sigma-Aldrich.

2.1 Modification of the diamonds with poly-L-lysine

To attach pLys to the surfaces of the diamonds, NV-COOH were suspended in DMF in 2% (w/w) concentration. The suspension was treated in the ultrasonic bath (Polsonic Sonic-3, 40 kHz) for 30 minutes to disaggregate the particles and homogenize their distribution. Next, 2.5 mL of the suspension and 100 µL of N,N'-Diisopropylcarbodiimide (DIC) were added to a flask containing 5 mg of previously lyophilized pLys. The reaction mixture was stirred overnight at room temperature. Then the desired solid product (NV-pLys) was obtained by centrifugation (5000 rpm, 5 min), washed with DMF, and then four times with methanol, every time being isolated by centrifugation and dried under a stream of air.

2.2 XPS

The elemental surface composition was determined by high-resolution X-ray photoelectron spectroscopy (XPS) with the monochromatic Al Kα source with pass energy 20 eV and 650 µm diameter spot size (Escalab 250Xi, ThermoFisher Scientific). Charge compensation was done using the Ar+ ions flood gun. Spectra were recorded

for C1s and N1s peaks. Normalization of binding energy for the peak characteristics of C1s (284.8 eV) was performed. The data analysis was performed using Avantage software provided by the manufacturer.

2.3 Preparation of the diamond suspensions with a wide pH range

To carry out statistical research on the precise influence of pH on the physical properties of NV centers contained in NV-COOH and NV-pLys, 11 solvents with integer values of pH in the range of 2.00–12.00 were prepared to serve as dispersion media for the diamonds. The solvents with pH from 2.00 to 6.00 were prepared by adding 0.1M HCl to deionized water, while the solvents with pH from 7.00 to 12.00 resulted from mixing deionized water with 0.1M NaOH. In each case, the volumes of water, and HCl or NaOH were chosen experimentally, while constantly monitoring the resulting pH of the solvent with the use of the Mettler Toledo pH meter equipped with the InLab Expert Pro-ISM electrode. An aqueous suspension of NV-COOH with 0.2% (w/w) concentration was subjected to the ultrasonic bath for 30 min, and then individually mixed with a portion of every one of the 11 solvents in 1:1 volume ratio, thus creating diamond suspensions with diverse pH and identical concentrations of the particles. Three identical suspensions were made from each of the 11 solvents. Dried diamonds modified with poly-L-lysine (NV-pLys) were dispersed in every one of the 11 solvents in 0.1% (w/v) concentration. The particles were disaggregated first in the ultrasonic bath for 45 min, and then with the ultrasonic homogenizer Bandelin Sonopuls HD 4200 equipped with TS 106 sonotrode. The homogenizer was adjusted to work in a pulsed mode with 0.5-second work step and 0.5-second idle step. Every NV-pLys suspension was homogenized for a total time of 10 minutes, which equals to 5 minutes of active transmission of the ultrasound. The resulting pH values of all prepared suspensions (NV-COOH and NV-pLys) have been measured and are summarized in Table 1.

Table 1. *pH values of the diamond suspensions.*

Suspension	pH of the solvent	pH of the suspension
NV-COOH 2	2	2.32
NV-COOH 3	3	3.34
NV-COOH 4	4	4.38
NV-COOH 5	5	5.37
NV-COOH 6	6	5.82
NV-COOH 7	7	6.53
NV-COOH 8	8	6.33
NV-COOH 9	9	6.41
NV-COOH 10	10	6.77
NV-COOH 11	11	10.27
NV-COOH 12	12	11.64

NV-pLys 2	2	2.30
NV-pLys 3	3	6.68
NV-pLys 4	4	7.77
NV-pLys 5	5	7.91
NV-pLys 6	6	7.55
NV-pLys 7	7	7.82
NV-pLys 8	8	7.94
NV-pLys 9	9	7.96
NV-pLys 10	10	8.62
NV-pLys 11	11	10.43
NV-pLys 12	12	11.93

2.4 Fluorescence measurements

Fluorescence spectra were measured by means of a custom-built laboratory setup equipped with a 532 nm laser excitation source (Nd:YAG SHG laser Millenia, Spectra Physics) operating at the power level of 0.2 W. The emission spectra were recorded utilizing a 0.3 m monochromator (SR303i, Andor) equipped with 600 groves/mm grating and ICCD detector (DH740, Andor). Samples were analyzed in a quartz cuvette excited with a laser beam at an angle of 45 degrees. The fluorescence was collected using a quartz lens end focused on the entrance of an optical fiber. The band-pass filter (OG570, Schott) was used in the detection path to eliminate the laser radiation. The solvents prepared to serve as dispersion media for the diamonds were examined first. The signals registered from the solvents could later be subtracted as background photoluminescence from the spectra of the diamond suspensions. Therefore, it was possible to present spectra depicting only the fluorescence coming from the diamonds themselves. Every suspension (NV-COOH and NV-pLys) was measured 3 times to check the stability of the intensity of the fluorescence over time. The time interval between successive measurements of the fluorescence for a single suspension has been set to 60 seconds.

2.5 Particle analysis

The zeta potential (ζ) of NV-COOH was measured in 2–12 pH range using the NanoBrook Omni analyzer equipped with the BI-ZTU Autotitrator (Brookhaven Instruments, USA). For this purpose, the diamonds had been suspended in 0.1M HCl. The zeta potential of the suspension was measured at its starting pH, and then the pH was being gradually increased while the analyzer was registering the values of ζ.

Particle size distributions and ζ of NV-pLys were examined in the broad range of pH using the Zetasizer Nano ZS analyzer (Malvern Panalytical, UK) equipped with a 632.8 nm laser and a narrowband filter (ZEN9062). The

suspensions were stirred at 500 rpm for 5 min using the VELP Scientifica TX4 digital vortex mixer prior to the measurements. Every suspension was placed in a high concentration cell (ZEN1010) and measured at 25°C using backscatter detection (173°) for particle size analysis, and forward detection (13°) for a determination of ζ.

Five measurements of the particle size distributions were taken for every suspension, with a single measurement consisting of 12 scans. The results were analyzed for the mean particle diameter aka Z-Average (d) and polydispersity index (PDI), both given by cumulants analysis of the scattered signal. Since PDI includes information on the standard deviation of the distribution[30], the value of PDI averaged from 5 measurements was used to determine the standard error of the mean. The measurements of ζ were repeated 5 times for every suspension, with a single measurement consisting of 22 scans.

2.6 Contact angle

Measurements of the contact angle of the tested suspensions were made by applying drops with a capacity of 2-4 µl on both Ti-6Al-4V and PTFE surfaces. Then, using a drop shape analyzer DSA100 (KRÜSS, Germany) equipped with a high-resolution camera, the measurements of the contact angle on both sides were made, repeating the measurement 30 times. The shape of the drop was modeled using ADVANCE software and the Young-Laplace method, obtaining contact angle results for all samples. Moreover, using the pendant drop method, the surface tension of the tested suspensions was measured[31,32]. An experiment was also carried out on diamonds-modified Ti-6Al-4V plates to determine the effect of deposited particles on wettability. A drop of about 15-20 µl was deposited on the plate and left for 15-20 minutes to dry. Then the water contact angle (pH=1.5; 7 and 11.5) on these spots was measured. In this way, we imitated the deposition of the particles when measuring the contact angle on the reference PTFE surface.

3. Results and discussion

3.1 Synthesis and molecular structure of pLys-functionalized diamonds

The synthesis of pLys-functionalized FDPs was carried out in dimethylformamide (DMF) used as a polar aprotic solvent. It is worth mentioning that utilized methodology including chosen set of solvents (Section 2.1) assures the absence of unreacted pLys at the FDPs' surface. To confirm the particles' surface modification and determine

the pLys structure, the NV-COOH, functionalized NV-pLys, as well as pLys itself, were characterized by FT-IR spectroscopy (Fig. 2A).

First, the FT-IR spectra of pLys, indicated by the green line, were characterized. The peak observed at 3430 cm^{-1} corresponds to the stretching vibrations of secondary amide and side-chain amine NH_2 groups. Next, the bands observed at 3288 cm^{-1} are associated with the stretching vibrations of charged side chain NH_3^+ groups[33]. At 3054 cm^{-1}, 2939 cm^{-1}, and 2856 cm^{-1} bands related to C-H stretching modes of C-H and CH_2 side chain groups can be observed. Moreover, at 1652 cm^{-1} and 1627 cm^{-1} the characteristic bands of the secondary amide group (O=C-NH-C) assigned to stretching vibrations are present. Based on the location of these bands, the random coils in the pLys structure can be suggested[34]. The band appearing at 1546 cm^{-1} corresponds to deformation vibrations of N-H groups present in the secondary amide group. Next, the bands appearing at 1394 cm^{-1} and 1176 cm^{-1} correspond to symmetrical bending and skeletal vibrations of the C-H group. Finally, the signal at 1207 cm^{-1} is associated with the stretching and vibrations of the C=O group.

Next, the FT-IR spectra of NV-COOH were analyzed (indicated by the black line). In this case, we could clearly distinguish three bands. First, the band observed at 3511 cm^{-1} is associated with the stretching vibrations of –OH groups [28]. Second, bands at 2924 cm^{-1} and 2854 cm^{-1} related to the CH_2 groups. Third, the band positioned at 1744 cm^{-1} is related to stretching vibrations of C=O groups [35].

The FT-IR spectra obtained for NV-pLys (indicated by the red solid line) indicate the effective functionalization with pLys. The intensity of the obtained IR bands clearly suggest the high efficiency of performed modification. Moreover, the broad absorption bands observed in the region from 3655 cm^{-1} to 3120 cm^{-1} may be associated with intramolecular hydrogen bonds occurring at the diamond's surface [35]. Furthermore, the band at 848 cm^{-1}, may be associated with the stretching vibrations of C–N present in FDPs' [36]. All the above facts confirm the presence of covalently attached pLys at the FDPs' surface.

The XPS analysis was performed to additionally determine the chemical composition of pLys-modified particles. High-resolution XPS spectra performed for C1s and N1s are shown in Fig. 2B, C, and E. The charge shift was corrected by referencing to the adventitious C1s peak at 284.8 eV. Five elementary peaks were proposed for the C1s spectrum and two for the N1s spectrum to perform deconvolution.

For carbon, deconvolution was used assuming the presence of sp2 and sp3 hybridized carbon and the C-O and C=O impurities in NV-COOH sample (Fig. 2B) [37]. In the case of the NV-pLys sample, the model had to be extended with an additional peak related to the presence of the NC=O groups [38]. The amino groups from pLys could be observed at an energy close to the C-O bond (285.7 eV) (Fig. 2C). A model with two forms of nitrogen (NH-C at an energy of 399.3 eV and NC=O at an energy of 401 eV) was achieved for NV-pLys revealing poly-L-lysine structure similarly to presented previously in [39] (Fig. 2E). No nitrogen was detected in the NV-COOH sample.

The interpretation of the peaks has been summarized in Fig. 2D where the atomic content of each form of carbon and nitrogen have been listed. In the NV-pLys sample, the content of carbon-nitrogen bonded species is considerably increased due to pLys presence. Changes between the bare and the functionalized samples clearly manifest that the FDP's surface was effectively functionalized with pLys.

3.2 Fluorescence studies of NV-pLys in the function of pH

All measurements have been conducted within the pH range 2-12. The range has been adjusted based mainly on the behaviour of pLys at different pHs and its pKa values which are equal to 2.18, 8.95 and 10.53. Based on these values and chosen immobilization method the changes in the pLys conformation below pH 2 and above pH 11 are not expected. Fig. 3A depicts fluorescence spectra emitted by the NV-COOH. Taking the readability of the graph into consideration, the spectra of every second sample are presented. Each spectrum has been averaged from 3 measurements. At the wavelength of 637 nm, all spectra have local extremes (as indicated in Fig. 3A), which are the zero-phonon lines (ZPLs) of the negatively charged nitrogen-vacancy centers. The 1^{st} and 2^{nd} phonon sidebands are also noticed as the next two local maxima in the spectra. As can be seen in Fig. 3A, the intensity of the emitted fluorescence increases along with increasing pH until it reaches a value of 6. This increase is related mainly to the dissociation of the carboxyl groups. These results correspond with observations of H. Raabova et. al. [18]. However, with the transition of the pH from acidic to alkaline, ZPLs' intensity decreases and is not variable up to pH 10. At pH values > 10 ZPLs' intensity slightly decreases, which may be associated with an increased amount of OH^- ions. Figure S1 in Supplementary information shows the photon counts registered at 637 nm (the zero-phonon line of NV- centers) plotted versus the initial pH of the dispersion media. Furthermore, a statistical analysis of the pH-induced changes has been carried out (Figure S2). Except for one result obtained for pH = 7, all the results fall within the reasonable extremes. The changes registered within both

acidic and alkaline ranges (excluding changes in the fluorescence intensity between pH = 9 and pH = 10 and between pH = 10 and pH = 11) are statistically significant ($p \leq 0.05$).

Fig. 3B depicts the fluorescence spectra of the NV-pLys suspensions in different pH values. First, what can be noticed is the overall decrease in the intensity of the signal. The two orders of magnitude drop comparing to the previous measurements presented in Fig. 3A can be attributed to the chemical functionalization and immobilized protein, which physically masks some functions of the particles. However, it can be also attributed to the cationic character of pLys, which led to a depletion of NV^- occupancy, thus decreasing its emission intensity. As in the previous case, the ZPLs of the NV^- centers, as well as the 1^{st} and 2^{nd} phonon sidebands, are visible. Except for the intensity changes we do not observe any shifts in the ZPLs. However, in contrast to the case of NV-COOH, the intensity of the fluorescence emitted by the NV^- centers vary with pH change, and therefore, based on these values no general trend can be identified. What needs to be emphasized is the fact that the final fluorescence signal in both investigated cases is a result of the surface charges and the pH of the surrounding environment.

To further elucidate the nature of this process, we have studied the NV^-/NV^0 ratio of intensities at NV^0 ZPL (575 nm), at NV^- ZPL (637 nm), and its dependence on pH (Fig. 3C). The ratio has been calculated by the readout of the maximum photon counts at the wavelength of 637 and 575 nm, and finally by dividing the obtained values. In terms of NV-COOH (black line), we can notice the monotonous decrease in the pH range from 2 to 8 which is mainly caused by the dissociation of the carboxyl groups and the presence of H^+ ions in the solution what results in the depletion of NV center. The transition of the pH from neutral to alkaline increases the value of the NV^-/NV^0 ratio. This, in turn, can be associated with the increased amount of OH^- radicals. The obtained results indicate that the pH changes can be monitored with the use of the NV^- color centers within the range of 2-7, which stays with the agreement to the work reported in [15]. However, taking into account the whole spectrum of pH, it can be noticed, that with the alkaline pH (7-10), the signal increases. The increase, in turn, takes place in the same range as the decrease in the acidic pH.

Unlike the carboxyl groups, in the case of NV-pLys, the net surface charge except for pH of the surrounding environment and groups on the particle's surface is also the result of immobilized pLys' charge and its conformation. First what can be seen is the overall drop of the intensity ratio, the same as can be observed in Fig. 3B. As a result of the pLys functionalization, the NV^- gets depopulated first (pH 2-3), shifting the charge state to NV^0. Although the net charge of the pLys on the NV-pLys surface was positive at the pH value equal to ~2, the

relaxed/extended conformation of the pLys did not cover the diamonds' surfaces, and thus, was not able to affect the NV centers. Only after a further change of the pH, when the conformation transformed into the more compressed one, drawing the positive charge closer to the particle surface, a significant reduction of the NV^-/NV^0 intensity ratio can be observed. Further increase of the pH along with conformational changes within the structure of pLys lead to increasing the NV^-/NV^0 intensity ratio, which indicated increasing visibility of NV centers. The alkaline pH shrinks the pLys to its limits therefore the pLys crown compressed covering tightly the FDPs. It needs to be mentioned that at pH higher than 10 the amino groups present in the side chain of the pLys lose their positive charge, while the negative one appears on the carboxyl groups. However, considering the way of pLys immobilization, the majority of carboxyl group are involved in anchoring the pLys at the FDPs' surface. Therefore, at higher pH (pH>10) the molecule loses its charge and acid-base properties what partially influence and lower the intensity. This effect may be further enhanced by the presence of the OH^- ions.

To conclude, the charge modulation of pLys covalently attached to the diamonds' surface indeed induced NV emission tuning increasing the responsiveness of the NV^- to the surrounding pH. It can be observed especially in the area between 7 and 12, where the bare NVs, or NV-COOH showed little or no changes as reported in [14,40]; or as in the presented case, the changes are very similar to those obtained between pH 2 and 7.

3.3 pH-induced surface charge modulation of NV-pLys: ζ and particle size measurements

Zeta potential (ζ) measurements were conducted to further investigate the variation of the surface charge of NV-COOH and NV-pLys as a function of pH and its influence on the stability of the particles (Fig. 4).

First, we have measured the zeta potential of NV-COOH. As can be seen in Fig. 4A, at low pH values the zeta potential oscillates around 0 mV and is gradually decreasing with increasing pH, reaching a minimum value of −27.09 mV at pH 11.55. The obtained results complement previously described fluorescence measurements and mirror the ionization process of the carboxylated diamonds' surface. The oxidized surface of NV is electroneutral in acidic solutions, which makes the diamonds unstable and prone to aggregation. Once the pH increases, H^+ ions become depleted from the solution as well as from the carboxyl groups present on the diamonds' surface, converting the particles into negatively charged and stabilizing them in the suspension, which is reflected by the negative ζ value.

Subsequently, NV-pLys were measured (see also Fig. 4B). What can be seen is the pLys has stabilized the diamonds over a wide range of pH, providing effective colloidal stability. The ζ values of investigated cases reached from 52.6 at pH 2, through 67.3 mV at pH 3, to approx. 54 mV for pH values ranging 4 to 10. With the increase of pH, the zeta potential is gradually decreasing reaching a minimum value of -12.8 mV at pH 12 with an isoelectric point around pH 11.5. Considering the structure of pLys, the positive ζ values at acidic pH indicate the protonation of the amino groups (NH_3^+) which originate only from immobilized pLys. The pLys carboxyl groups (COOH), in turn, are fully protonated at low pH, thus they are noncharged. With increasing pH, the negative ζ values are attributed mainly to the deprotonation of carboxyl (COO^-) and amine groups (NH_2). In the case of the carboxyl groups, they can originate from both immobilized pLys as well as from free COOH groups on the diamond's surface. However, as it was mentioned in the previous Section, most of pLys' carboxyl groups are involved in anchoring the pLys at the FDPs' surface. Therefore, at higher pH (pH>10) the molecule loses its charge and acid-base properties what results in stability loss.

Besides the ζ measurements, we have also conducted the dynamic light scattering (DLS) analysis – to additionally prove the stabilization of the NV-pLys functionalization. Figure 4B shows the mean particle size in the function of pH (blue). Particles suspended in the solutions with the pH ranging from 2 to 10 show outstanding stability with a mean particle size of approx. 712.44 nm what stays in agreement with a claimed average particle size of utilized particles (Methods). Once the pH of the suspension has been changed to 11 and 12, particles reveal significant agglomeration with aggregate sizes on the order of 1347.20 and 2029.20 nm for pH equal 11 and 12, respectively.

3.4 Interactions of NV-pLys particles with surfaces

It is known that the presence of nanoparticles in the solution affects wettability and reduces the interfacial tension (IFT) [42]. Wettability, in turn, is an important parameter that allows determining the biocompatibility of the tested particles but also their interactions with different kinds of materials, which is of big importance in the case of enhancing the properties of, e.g., implants. Therefore, we assessed a wide range of parameters based on the phenomenon of wettability, the assessment of which will allow for a full characterization of the presented structures in the context of their potential use as biomedical surfaces, as well as the impact of pLys modification on this process. The parameters of the surface tension (SFT) and the contact angle (CA) (on PTFE) of diamond

suspensions with different pH allowed to determine the surface free energy (SFE) with its components - disperse and polar (Fig. 5).

The NV-COOH has shown a significant increase in hydrophobicity when switching from acidic to basic pH (Fig. 5A – indicated by the black points). The NV-COOH at pH 3 was characterized by the lowest value of the CA (94.75°±0.94), and the highest value was registered for the NV-COOH at pH 12 (111.11°±0.37). The NV-pLys (Fig. 5A indicated by the red points) shown an exactly opposite relationship - an increase in hydrophilicity with an (89.89°±0.29) was registered for pH 9, whereas the highest was recorded at pH 3 (100.62°±0.55).

What is also important to notice, surface tension (Fig. 5B) and surface free energy (Fig. 5C) take higher values for NV-pLys. These values vary with pH change; therefore, no general trend can be established. If we look at the individual elements of the surface free energy (Fig. 5D), there is a large variation between the studied particles. NV-COOH are essentially characterized by similar values of the disperse (γ^D) and polar (γ^P) parts, with one of these parts dominating only at extreme pH values (pH 2 and 12). On the other hand, NV-pLys mostly show high values of the dispersion part with minimal polar part, indicating that most of the interactions are dispersive (van der Waals, Keesom, Debye, London interactions). The polar part corresponds to Lewis's acid-base interactions and hydrogen bonds. The parameters except for determining the dominant type of interactions, perfectly mirror the properties of functional groups present on the surface of investigated particles. Moreover, these values are an important indicator showing the possibility of interaction with other individuals, such as organic and inorganic analytes in sensory systems, as well as tissue components, in the case of materials with biomedical application [31,43]. However, to determine if the two elements will interact, parameters such as the work of adhesion (WoA) and the spreading coefficient (S) are needed (Fig. 6).

The values of the WoA obtained for all NV-pLys suspensions differ in the range from about 76 to 99 mN/m. The highest values are for samples with pH 4-10, and the lowest for pH 12. As for the spreading coefficient (S), there are only slight changes visible, and the negative values of which indicate poor wetting of the tested surfaces. Here, too, the sample with pH 12 has the lowest value, while, interestingly, the highest value is pH 11. Differences in IFT between these suspensions in the range of pH 2-10 gradually decrease. However, in the case of a sample with pH 11, it is a significant change in this parameter and a sudden increase up to the value of 25.67 mN/m. Such variability of this parameter indicates a different degree of long-term adhesion of these suspensions

but may also be the result of their different durability. Samples with pH 11 and 12 showed very low stability (Fig. 4), and the particles sedimented very quickly, which may explain the irregularities in the obtained results.

Subsequently investigated Ti-6Al-4V alloy is characterized practically only by its dispersion mode of interaction, so polar interactions contribute negligibly to the reduction of IFT. Hence poor wetting and high contact angle. Comparing the obtained results with the results obtained on PTFE, which is also a fully dispersive material (γ^S = 20 mN/m, γ^D = 18.4 mN/m, γ^P = 1.6 mN/m), we see that the tested systems generally show lower interfacial tension, probably due to a slightly higher proportion of polar interactions. Lower values indicate better long-term adhesion for the Ti-6Al-4V sample than for PTFE. Comparing the results obtained for NV-COOH and NV-pLys, we can see that the latter are much less sensitive to changes in pH. On the other hand, the changing trend itself is the opposite of that in the case of nonmodified nanoparticles. This is evident, for example, when considering the changes in IFT/calc. CA vs. pH. NV-COOH are characterized by an increasing value of the interfacial tension going from acidic to basic pH. In addition, we also see an increase in the calc. CA value. Initially, the values oscillate slightly below 90°, and in a strongly alkaline environment, they are close to 100°. On the other hand, in the case of the WoA parameters and the S, the values for the modified particles are higher by approx. 10-40% for WoA and 5-20% for S, and these values increase with increasing pH. This increase is significantly higher for nonmodified particles. The observed differences in the behavior of NV-pLys particles are caused on the one hand by the chemical nature of the groups present on the surface of these diamonds, but also by the buffer capacity of the presented structures.

Next, the wettability of the plates with deposited diamonds was measured in three different pH values – key values for pLys relating to its three ionization states (Fig. 7).

The obtained results show a significant influence of the deposition of the particles on the observed surface CA, both in the case of NV-COOH and NV-pLys (Fig. 7). The deposition of the FDPs on the surface of the material undoubtedly affects its wettability. In the case of NV-COOH (Fig. 7A), the CA is the highest (79.57°±0.82) for the lowest pH because of the carboxyl groups' protonation. At higher pH, the CA drops to 60.24°±0.84 due to the ionization of the carboxyl group what makes the surface much more hydrophilic. Although we were expecting a further decrease in the CA through the ionization of carboxyl groups, the CA increased reaching the value of 71.68°±1.75 at pH 10. This change could be attributed to the electrostatic attraction between the negatively charged diamond surface and the compensating protons in the aqueous film [44].

Nevertheless, the most significant changes are visible for NV-pLys (Fig. 7B). Considering fluctuations corresponding to the experimental errors it can be stated that pLys-functionalized diamonds are not affected by the pH changes. In all measured pH, the NV-pLys lowered the CA to ~ 35° which is ca. 57% less than for the blank sample (TiAlV plate). It is worth noting that in the case of NV-COOH these changes did not exceed 20%. In the NV-pLys case, the CA greatly reflects the influence of pH on the ionization of the pLys functional groups at the diamonds' surface. At low pH, the CA of solvents is determined mostly by amino groups which are all in NH^{3+} form. As the pH of the droplet increases, the amino groups begin to lose their charge, however, at the same time, the ionization of carboxyl groups begins, therefore stabilizes the CA. The stable and highly improved hydrophilicity of the material may directly correspond to their improved biocompatibility.

4. Conclusions

To summarize, we have successfully performed the carboxylated fluorescent diamond particles' (FDPs') modification with poly-L-Lysine in an anhydrous medium, which was confirmed by XPS and FT-IR spectroscopy. Next, we have analyzed the fluorescence specifically exhibited by the NV^- defects embedded in the FDP structure within a wide pH range. What turned out, the surface charge modulation, i.e., modification of the diamonds' surface with pLys, changed its response, thereby the measurable pH range. Surface charge modulations were further analyzed by the means of the zeta potential, particle size, as well as contact angle measurements. Our results suggest that the modification with pLys – except for changes in the range of the responsiveness in terms of pH measurements – firstly, provides high aggregation control, and long-term stability over a wide range of pH. Secondly, the improvement of wetting properties may also increase NV-pLys biocompatibility. This indirect tuning of the interactions between FDPs and biofluids prepares the diamonds to work in the cellular environment, e.g., as a part of an implant, favoring early stages of cell adhesion. Moreover, free functional groups of pLys could be also further utilized as a binding site aiming at, for example, the loading of bioactive compounds, such as pro-osteogenic agents, drugs preventing bone resorption, or implant-related inflammation/infections.

Conflicts of interest

There are no conflicts to declare.

Acknowledgements

This research work is supported by the National Science Centre, Poland under grant no. 2016/21/B/ST7/01430, and the Foundation for Polish Science within the „TEAM-NET" project carried out within the POIR.04.04.00-00-1644/18 programme co-financed by the European Union under the European Regional Development Fund. R. Bogdanowicz gratefully acknowledges financial support from the National Science Centre under project No. UMO-2020/01/0/ST7/00104. M. Janik acknowledges the support from the Foundation for Polish Science within the START 2021 program. The Authors would like to gratefully acknowledge Mr. Raffaele Carano and Mr. Carlo Dessy from Testa Analytical Solutions (Germany) for carrying out the measurements of the zeta potential of carboxylated diamonds.

Data availability

Data supporting the findings of this study are available within the and from the corresponding authors upon reasonable request.

References

[1] N. Nunn, M. Torelli, G. Mcguire, O. Shenderova, Nanodiamond : A high impact nanomaterial, Curr. Opin. Solid State Mater. Sci. 21 (2017) 1–9. https://doi.org/10.1016/j.cossms.2016.06.008.

[2] Y. Ruan, D.A. Simpson, J. Jeske, H. Ebendorff-he, W. Desmond, M. Lau, H. Ji, B.C. Johnson, T. Ohshima, S.A. V, A.D. Greentree, T.M. Monro, B.C. Gibson, Magnetically sensitive nanodiamond-doped tellurite glass fibers, Sci. Rep. 8 (2018) 1–6. https://doi.org/10.1038/s41598-018-19400-3.

[3] S. Hsieh, P. Bhattacharyya, C. Zu, T. Mittiga, T.J. Smart, F. Machado, B. Kobrin, N.Z. Rui, M. Kamrani, S. Chatterjee, S. Choi, M. Zaletel, V. V Struzhkin, J.E. Moore, V.I. Levitas, R. Jeanloz, N.Y. Yao, Imaging stress and magnetism at high pressures using a nanoscale quantum sensor, Science (80-.). 366 (2019) 1349–1354.

[4] G. Kucsko, P.C. Maurer, N.Y. Yao, M. Kubo, H.J. Noh, P.K. Lo, H. Park, M.D. Lukin, Nanometre-scale thermometry in a living cell, Nature. 500 (2013) 4–9. https://doi.org/10.1038/nature12373.

[5] Y. Wu, N.A. Alam, P. Balasubramanian, A. Ermakova, S. Fischer, H. Barth, M. Wagner, M. Raabe, F. Jelezko, T. Weil, Nanodiamond Theranostic for Light-Controlled Intracellular Heating and Nanoscale Temperature Sensing, Nano Lett. 21 (2021) 3780–3788. https://doi.org/10.1021/acs.nanolett.1c00043.

[6] G. Reina, L. Zhao, A. Bianco, N. Komatsu, Chemical Functionalization of Nanodiamonds: Opportunities and Challenges Ahead, Angew. Chemie - Int. Ed. 58 (2019) 17918–17929. https://doi.org/10.1002/anie.201905997.

[7] Z. Mi, C. Chen, H.Q. Tan, Y. Dou, C. Yang, S.P. Turaga, M. Ren, S.K. Vajandar, G.H. Yuen, T. Osipowicz, F. Watt, A.A. Bettiol, Quantifying nanodiamonds biodistribution in whole cells with correlative iono-nanoscopy, Nat. Commun. 12 (2021) 1–9. https://doi.org/10.1038/s41467-021-25004-9.

[8] W.W. Hsiao, Y.Y. Hui, P. Tsai, H. Chang, Fluorescent Nanodiamond : A Versatile Tool for Long-Term Cell Tracking , Super-Resolution Imaging , and Nanoscale Temperature Sensing, Acc. Chem. Res. 49 (2016) 400–407. https://doi.org/10.1021/acs.accounts.5b00484.

[9] X. Wu, M. Bruschi, T. Waag, S. Schweeberg, Y. Tian, T. Meinhardt, R. Stigler, K. Larsson, M. Funk, D. Steinmüller-Nethl, M. Rasse, A. Krueger, Functionalization of bone implants with nanodiamond particles and angiopoietin-1 to improve vascularization and bone regeneration, J. Mater. Chem. B. 5

(2017) 6629–6636. https://doi.org/10.1039/c7tb00723j.

[10] L. Grausova, L. Bacakova, A. Kromka, S. Potocky, M. Vanecek, M. Nesladek, V. Lisa, Nanodiamond as Promising Material for Bone Tissue Engineering, J. Nanosci. Nanotechnol. 9 (2009) 3524–3534. https://doi.org/10.1166/jnn.2009.NS26.

[11] J.R. Casey, S. Grinstein, J. Orlowski, Sensors and regulators of intracellular pH, Nat. Rev. Mol. Cell Biol. 11 (2009) 50–61. https://doi.org/10.1038/nrm2820.

[12] J. Jo, C.H. Lee, R. Kopelman, X. Wang, In vivo quantitative imaging of tumor pH by nanosonophore assisted multispectral photoacoustic imaging, Nat. Commun. 8 (2017). https://doi.org/10.1038/s41467-017-00598-1.

[13] F. Yu, O. Addison, S.J. Baker, A.J. Davenport, Lipopolysaccharide inhibits or accelerates biomedical titanium corrosion depending on environmental acidity, Int. J. Oral Sci. 7 (2015) 179–186. https://doi.org/10.1038/ijos.2014.76.

[14] M. Fujiwara, R. Tsukahara, Y. Sera, H. Yukawa, Y. Baba, S. Shikata, H. Hashimoto, Monitoring spin coherence of single nitrogen-vacancy centers in nanodiamonds during pH changes in aqueous buffer solutions, RCS Adv. 9 (2019) 12606–12614. https://doi.org/10.1039/c9ra02282a.

[15] T. Fujisaku, R. Tanabe, S. Onoda, R. Kubota, T.F. Segawa, T. Ohshima, I. Hamachi, M. Shirakawa, R. Igarashi, pH Nanosensor Using Electronic Spins in Diamond, ACS Nano. 13 (2019) 11726–11732. https://doi.org/10.1021/acsnano.9b05342.

[16] M. Sow, H. Steuer, S. Adekanye, L. Ginés, S. Mandal, B. Gilboa, O.A. Williams, J.M. Smith, A.N. Kapanidis, High-Throughput Detection and Manipulation of Single Nitrogen- Vacancy Center ' s Charge in Nanodiamonds, Arxiv. (2019) 1–42.

[17] T. Rendler, J. Neburkova, O. Zemek, J. Kotek, A. Zappe, Z. Chu, P. Cigler, J. Wrachtrup, Optical imaging of localized chemical events using programmable diamond quantum nanosensors, Nat. Commun. 8 (2017). https://doi.org/10.1038/ncomms14701.

[18] H. Raabova, D. Chvatil, P. Cigler, Diamond nano-optode for fluorescent measurements of pH and temperature, Nanoscale. 29 (2019) 18537–18542. https://doi.org/10.1039/c9nr03710a.

[19] R.A. Gittens, L. Scheideler, F. Rupp, S.L. Hyzy, J. Geis-gerstorfer, Z. Schwartz, B.D. Boyan, A review on the wettability of dental implant surfaces II : Biological and clinical aspects, ACTA Biomater. 10 (2014) 2907–2918. https://doi.org/10.1016/j.actbio.2014.03.032.

[20] V. Vaijayanthimala, Y.K. Tzeng, H.C. Chang, C.L. Li, The biocompatibility of fluorescent nanodiamonds and their mechanism of cellular uptake, Nanotechnology. 20 (2009). https://doi.org/10.1088/0957-4484/20/42/425103.

[21] E.K. Chow, E.K. Chow, X. Zhang, M. Chen, R. Lam, E. Robinson, H. Huang, D. Schaffer, E. Osawa, A. Goga, D. Ho, Nanodiamond Therapeutic Delivery Agents Mediate Enhanced Chemoresistant Tumor Treatment, Sci. Transl. Med. 3 (2011). https://doi.org/10.1126/scitranslmed.3001713.

[22] Y. Xing, W. Xiong, L. Zhu, E. Osawa, S. Hussin, L. Dai, DNA Damage in Embryonic Stem Cells Caused by Nanodiamonds, ACS Nano. 5 (2011) 2376–2384. https://doi.org/10.1021/nn200279k.

[23] X. Zhang, J. Yin, C. Kang, J. Li, Y. Zhu, W. Li, Q. Huang, Z. Zhu, Biodistribution and toxicity of nanodiamonds in mice after intratracheal instillation, Toxicol. Lett. 198 (2019) 237–243. https://doi.org/10.1016/j.toxlet.2010.07.001.

[24] D.R. Tasat, M.E. Bruno, M. Domingo, P. Gurman, O. Auciello, L. Paparella, P. Evelson, B. Guglielmotti, D.G. Olmedo, Biokinetics and tissue response to ultrananocrystalline diamond nanoparticles employed as coating for biomedical devices, J. Biomed. Mater. Res. B Appl. Biomater. 00B (2016) 1–8. https://doi.org/10.1002/jbm.b.33777.

[25] N. Daum, C. Tscheka, A. Neumeyer, M. Schneider, Novel approaches for drug delivery systems in nanomedicine : effects of particle design and shape, WIREs Nanomedicine and Nanobiotechnology. 4

(2012) 52–65. https://doi.org/10.1002/wnan.165.

[26] D. Zhang, Y. Zhang, L. Zheng, Y. Zhan, L. He, Graphene oxide / poly- L -lysine assembled layer for adhesion and electrochemical impedance detection of leukemia K562 cancer cells, Biosens. Bioelectron. 42 (2013) 112–118. https://doi.org/10.1016/j.bios.2012.10.057.

[27] R. Kaur, J.M. Chitanda, D. Michel, J. Maley, F. Borondics, P. Yang, R.E. Verrall, I. Badea, Lysine-functionalized nanodiamonds: Synthesis, physiochemical characterization, and nucleic acid binding studies, Int. J. Nanomedicine. 7 (2012) 3851–3866. https://doi.org/10.2147/IJN.S32877.

[28] L.C.L. Huang, H.C. Chang, Adsorption and immobilization of cytochrome c on nanodiamonds, Langmuir. 20 (2004) 5879–5884. https://doi.org/10.1021/la0495736.

[29] S. Alwani, R. Kaur, D. Michel, J.M. Chitanda, R.E. Verrall, C. Karunakaran, I. Badea, Lysine-functionalized nanodiamonds as gene carriers: Development of stable colloidal dispersion for in vitro cellular uptake studies and siRNA delivery application, Int. J. Nanomedicine. 11 (2016) 687–702. https://doi.org/10.2147/IJN.S92218.

[30] N. Raval, R. Maheshwari, D. Kalyane, S.R. Youngren-ortiz, M.B. Chougule, R.K. Tekade, Importance of Physicochemical Characterization of Nanoparticles in Pharmaceutical Product Development, Elsevier Inc., 2019. https://doi.org/10.1016/B978-0-12-817909-3.00010-8.

[31] T. Dąbrowa, A. Wcisło, W. Majstrzyk, P. Niedziałkowski, T. Ossowski, W. Więckiewicz, T. Gotszalk, Adhesion as a component of retention force of overdenture prostheses-study on selected Au based dental materials used for telescopic crowns using atomic force microscopy and contact angle techniques, J. Mech. Behav. Biomed. Mater. 121 (2021). https://doi.org/10.1016/j.jmbbm.2021.104648.

[32] A. Wcisło, J. Ryl, R. Bogdanowicz, A. Cirocka, D. Zarzecza, B. Finke, T. Ossowski, Tuning of the electrochemical properties of transparent fl uorine- doped tin oxide electrodes by microwave pulsed-plasma polymerized allylamine, Electrochim. Acta. 313 (2019) 432–440. https://doi.org/10.1016/j.electacta.2019.05.046.

[33] M. Rozenberg, G. Shoham, I. Reva, R. Fausto, A correlation between the proton stretching vibration red shift and the hydrogen bond length in polycrystalline amino acids and peptides, Phys. Chem. Chem. Phys. 7 (2005) 2376–2383.

[34] M. Rozenberg, G. Shoham, FTIR spectra of solid poly- L -lysine in the stretching NH mode range, Biophys. Chem. 125 (2007) 166–171. https://doi.org/10.1016/j.bpc.2006.07.008.

[35] T. Ando, K. Yamamoto, M. Ishii, M. Kamo, Y. Sato, Vapour-phase Oxidation of Diamond Surfaces in O2, studied by Diffuse Reflectance Fourier-transform Infrared and Temperature-programmed Desorption Spectroscopy, J. Chem. Soc. Faraday Trans. 89 (1993) 3635–3640.

[36] V.Y. Dolmatov, I.I. Kulakova, V. Myllymäki, A. Vehanen, A.A. Bochechka, A.N. Panova, B.T.T. Nguyen, IR Spectra of Diamonds of Different Origins and upon Different Purification Procedures, TOOLS, POWDERS, PASTES. 38 (2016) 58–65. https://doi.org/10.3103/S1063457616010093.

[37] F. Y. Xie et al. Surface characterization on graphitizationof nanodiamond powder annealed in nitrogen ambient, Surf. Interface Anal. 42 (2010) 1514-1518.

[38] M. Ariraman, R. Sasikumara, and M. Alagar, Shape memory effect on the formation of oxazoline and triazine rings of BCC/DGEBA copolymer RSC Adv. 5 (2015) 69720-69727.

[39] P. Niedziałkowski et al. Poly-l-lysine-modified boron-doped diamond electrodes for the amperometric detection of nucleic acid bases, J. Electroanal. Chem. 756 (2015) 84-93.

[40] V. Petrakova, I. Rehor, J. Stursa, M. Ledvina, M. Nesladek, P. Cigler, Charge-sensitive fluorescent nanosensors created from nanodiamonds, Nanoscale. 7 (2015) 12307–12311. https://doi.org/10.1039/c5nr00712g.

[41] L. Ginés, S. Mandal, C. Cheng, M. Sow, O.A. Williams, Positive zeta potential of nanodiamonds,

Nanoscale. 9 (2017) 12549–12555. https://doi.org/10.1039/c7nr03200e.

[42] S.O. Olayiwola, M. Dejam, A comprehensive review on interaction of nanoparticles with low salinity water and surfactant for enhanced oil recovery in sandstone and carbonate reservoirs, Fuel. 241 (2019) 1045–1057. https://doi.org/10.1016/j.fuel.2018.12.122.

[43] P. Niedziałkowski, M. Bojko, J. Ryl, A. Wcisło, M. Spodzieja, K. Magiera-mularz, K. Guzik, G. Dubin, T.A. Holak, T. Ossowski, Ultrasensitive electrochemical determination of the cancer biomarker protein sPD-L1 based on a BMS-8-modified gold electrode, Bioelectrochemistry. 139 (2021) 1–10. https://doi.org/10.1016/j.bioelechem.2021.107742.

[44] V. Chakrapani, J.C. Angus, A.B. Anderson, S.D. Wolter, B.R. Stoner, G.U. Sumanasekera, Charge Transfer Equilibria Between Diamond and an Aqueous Oxygen Electrochemical Redox Couple, Science (80-.). 318 (2007). https://doi.org/10.1126/science.1148841.

Figures

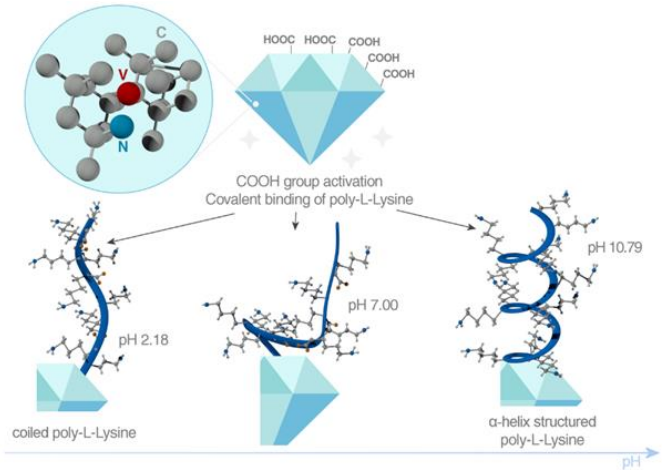

Fig. 1 *The explanatory model of poly-L-Lysine (pLys) attached to the diamond containing NV^- color centers, and changes in the pLys conformation depending on pH of the medium. Features are not to scale.*

a)

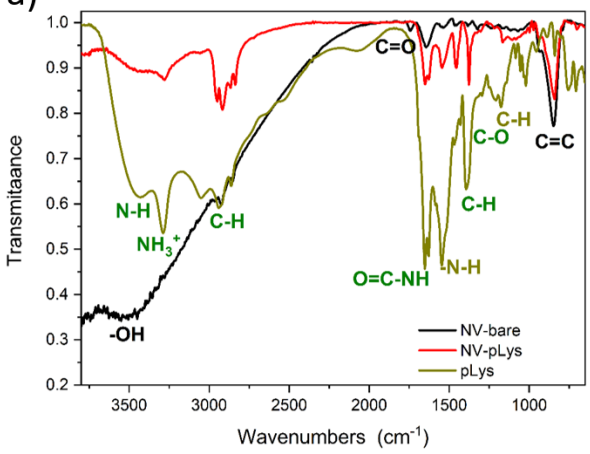

b)

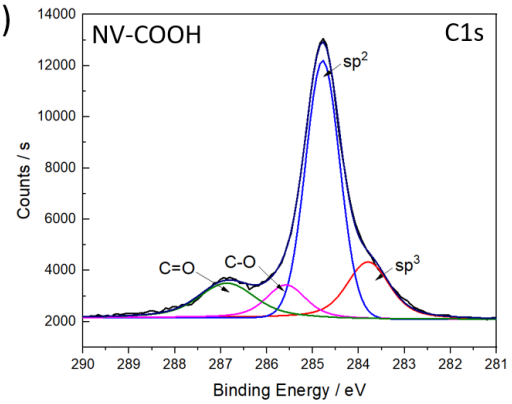

c)

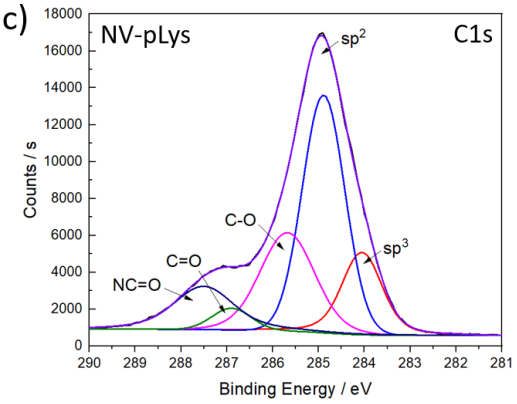

d)

	C1s sp^2	C1s sp^3	C1s C-O/C-N*	C1s C=O	C1s NC=O	N1s NC=O	N1s NH-C
NV-COOH	18.39	57.26	9.78	14.57	-	-	-
NV-pLys	14.18	39.55	21.44	3.29	11.27	3.17	6.59

e)

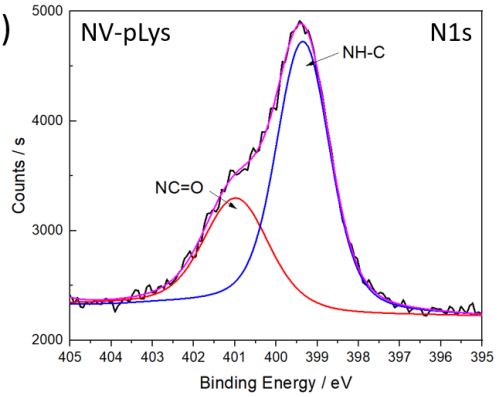

Fig. 2 *a) FT-IR spectra of 1) NV-COOH, 2) functionalized NV-pLys, and 3) pLys itself; High resolution XPS spectra of the C1s peaks of b) the nonmodified, carboxylated diamond samples (NV-COOH) and c) pLys-modified-diamond suspensions (NV-pLys); e) the N1s peak of NV-pLys; d) Atomic composition of the NV-COOH and the NV-pLys.*

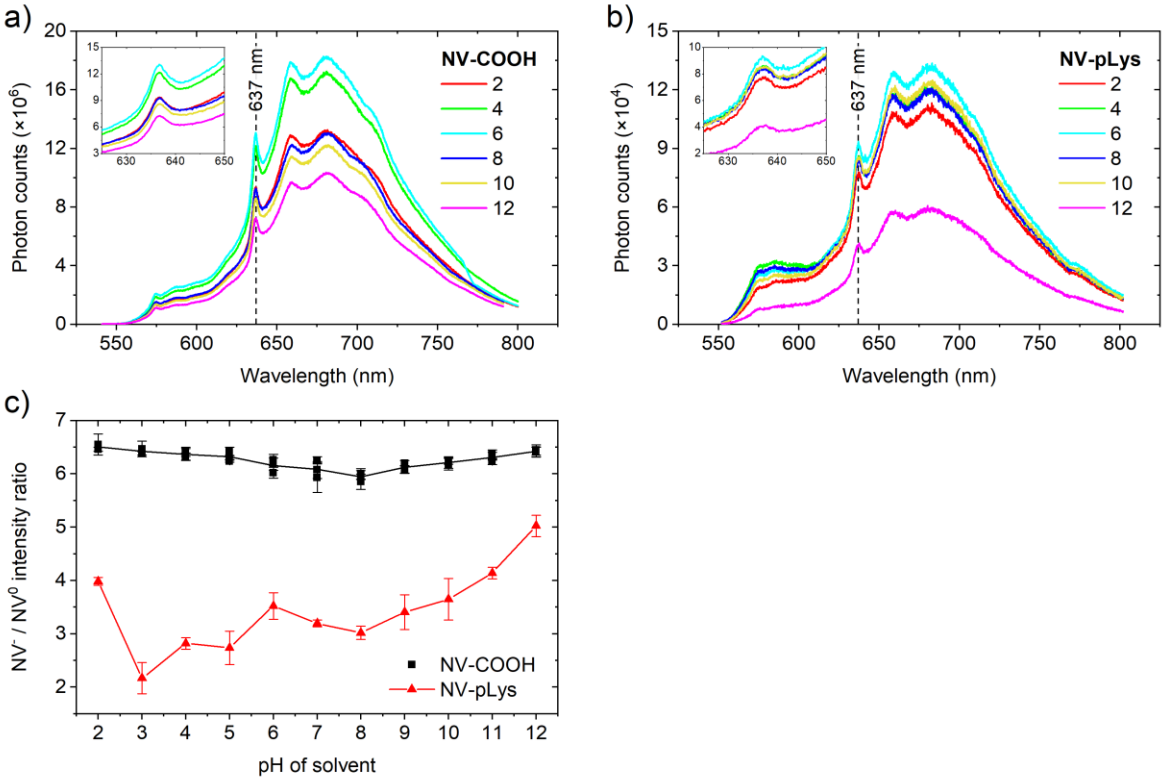

Fig. 3 *a) Fluorescence spectra of the nonmodified, carboxylated diamond suspensions (NV-COOH) and b) pLys-modified-diamond suspensions (NV-pLys); c) NV^-/NV^0 fluorescence intensity ratio of NV-COOH and NV-pLys for increasing pH. Error bars represent sample standard deviations from three measurements.*

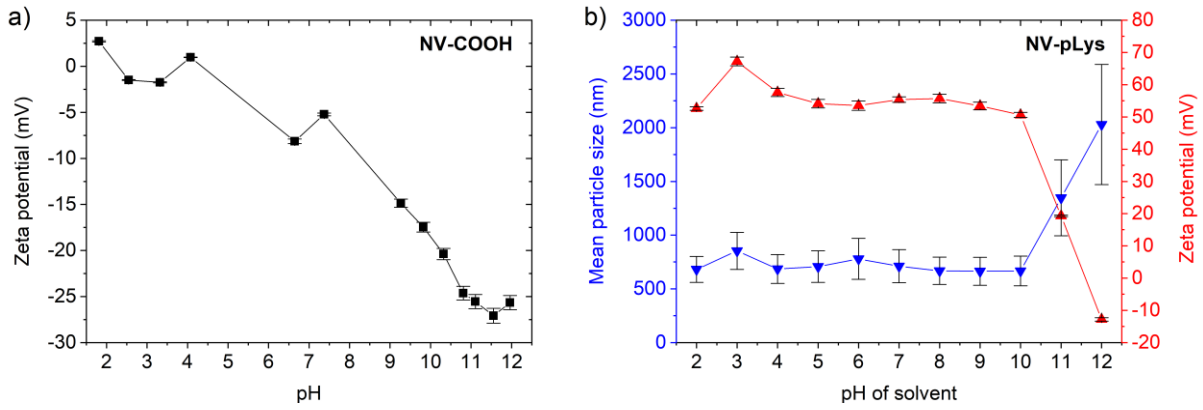

Fig. 4 *a) Zeta potential vs. pH for nonmodified, carboxylated diamond suspensions (NV-COOH), and b) Zeta potential (red) and mean particle size (blue) vs. pH for pLys-modified-diamond suspensions (NV-pLys).*

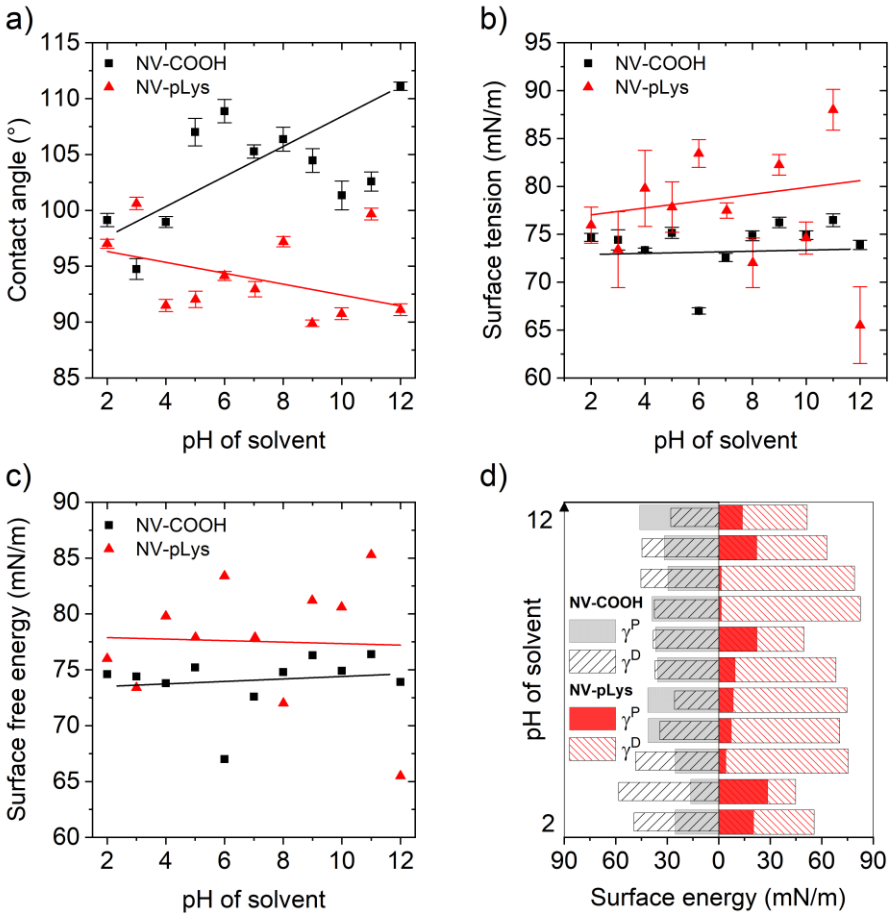

Fig. 5 *a) Contact angle (CA), b) surface tension (SFT), c) surface free energy (SFE) and d) its polar and disperse components of diamond vs. pH for nonmodified, carboxylated diamond suspensions (NV-COOH) and pLys-modified-diamond suspensions (NV-pLys) measured on the reference PTFE.*

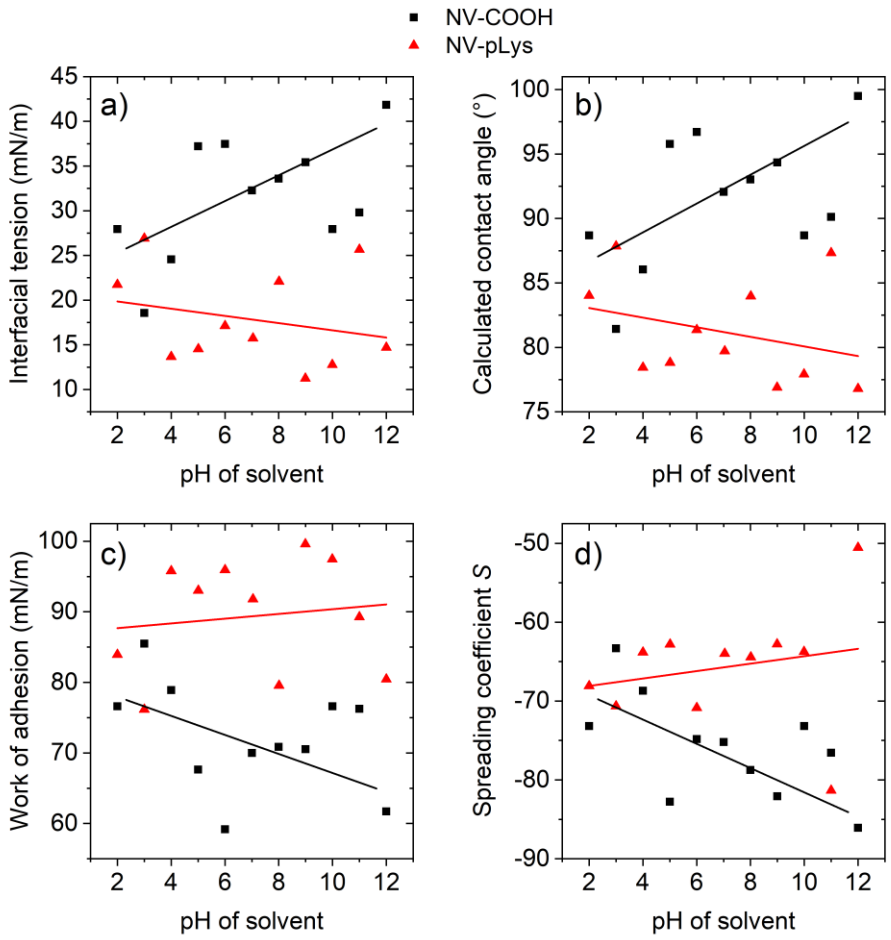

Fig. 6 *a) Interfacial tension (IFT); b) calculated contact angle values (Calc CA); c) work of adhesion (WoA), and d) spreading coefficient (S) of diamond vs. pH for nonmodified, carboxylated diamond suspensions (NV-COOH) and pLys-modified-diamond suspensions (NV-pLys) measured on the reference PTFE.*

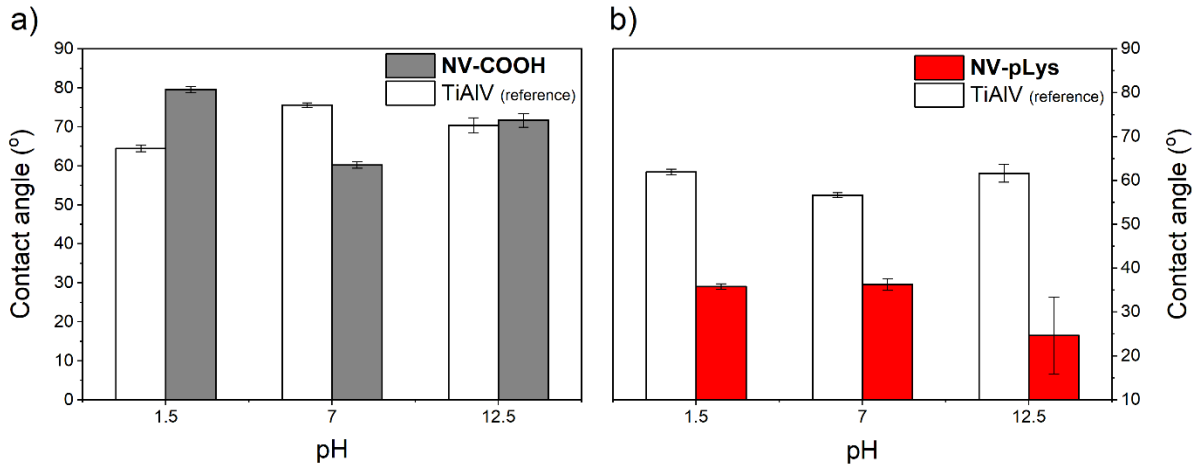

Fig. 7 *Wetting properties of Ti-6Al-4V surfaces vs. pH for the deposited A) nonmodified, carboxylated diamond suspensions (NV-COOH) and (b) pLys-modified-diamond suspensions (NV-pLys).*